

Article

# Nanostructured Chitosan/Maghemite Composites Thin Film for Potential Optical Detection of Mercury Ion by Surface Plasmon Resonance Investigation

Nurul Illya Muhamad Fauzi <sup>1</sup>, Yap Wing Fen <sup>1,2,\*</sup> , Nur Alia Sheh Omar <sup>2</sup>, Silvan Saleviter <sup>2</sup> , Wan Mohd Ebtisyam Mustaqim Mohd Daniyal <sup>2</sup>, Hazwani Suhaila Hashim <sup>1</sup> and Mohd Nasrullah <sup>3</sup>

<sup>1</sup> Department of Physics, Faculty of Science, Universiti Putra Malaysia, UPM Serdang 43400, Selangor, Malaysia; illyafauzi97@gmail.com (N.I.M.F.); hazwanisuhaila@gmail.com (H.S.H.)

<sup>2</sup> Functional Devices Laboratory, Institute of Advanced Technology, Universiti Putra Malaysia, UPM Serdang 43400, Selangor, Malaysia; nuralia.upm@gmail.com (N.A.S.O.); silvansaleviter94@gmail.com (S.S.); wanmdsyam@gmail.com (W.M.E.M.M.D.)

<sup>3</sup> Faculty of Civil Engineering Technology, Universiti Malaysia Pahang (UMP), Gambang 26300, Kuantan, Pahang, Malaysia; nasrul.ump@gmail.com

\* Correspondence: yapwingfen@gmail.com or yapwingfen@upm.edu.my

Received: 26 May 2020; Accepted: 12 June 2020; Published: 4 July 2020



**Abstract:** In this study, synthesis and characterization of chitosan/maghemite (Cs/Fe<sub>2</sub>O<sub>3</sub>) composites thin film has been described. Its properties were characterized using Fourier transform infrared spectroscopy (FTIR), atomic force microscopy (AFM) and ultraviolet-visible spectroscopy (UV-Vis). FTIR confirmed the existence of Fe–O bond, C–N bond, C–C bond, C–O bond, O=C=O bond and O–H bond in Cs/Fe<sub>2</sub>O<sub>3</sub> thin film. The surface morphology of the thin film indicated the relatively smooth and homogenous thin film, and also confirmed the interaction of Fe<sub>2</sub>O<sub>3</sub> with the chitosan. Next, the UV-Vis result showed high absorbance value with an optical band gap of 4.013 eV. The incorporation of this Cs/Fe<sub>2</sub>O<sub>3</sub> thin film with an optical-based method, i.e., surface plasmon resonance spectroscopy showed positive response where mercury ion (Hg<sup>2+</sup>) can be detected down to 0.01 ppm (49.9 nM). These results validate the potential of Cs/Fe<sub>2</sub>O<sub>3</sub> thin film for optical sensing applications in Hg<sup>2+</sup> detection.

**Keywords:** chitosan; maghemite; optical; mercury ion; surface plasmon resonance

## 1. Introduction

Organic polymeric materials made up of many repeating monomer units have made a significant impact on biological and biomedical research activities because of the flexibility and the ease of fabrication [1]. One of the well-known organic polymeric materials is chitosan, easily derived from partial deacetylation of chitin with a degree of 50% or greater [2–4]. To be more specific, chitosan is a family of linear polysaccharide as a part of glucosamine and N-acetyl glucosamine units linked via β-1,4 glucosidic bonds [5,6]. Chitosan contains three types of reactive functional groups, primary amine groups and primary and secondary hydroxyl groups, respectively, at positions C-2, C-3 and C-6. Among the three types of functional groups, the primary amine groups at C-2 positions are the most favorable sites interacting with the biological molecules, metal ions and organic halogen substances. Taking the advantages of chitosan with high absorption capacity and high biocompatibility, chitosan is known as an ideal substrate for enzyme immobilization [7]. Other excellent advantages of chitosan including non-toxicity, great film-forming ability, powerful adhesion property and high mechanical strength, offers great room for sensor applications [8–10]. However, the problem of poor stableness

of chitosan because of the hydrophilic character and pH sensitivity restricts its application [11,12]. Previous reports showed that the stability of chitosan could be improved by combining with oxide or metal oxides and the product can be effectively used as recognition elements for chemical sensors and biosensors [13–15].

Iron (III) oxide or ferric oxide is the inorganic compound with the  $\text{Fe}_2\text{O}_3$  formula, which varies in color depending on its phase [16].  $\text{Fe}_2\text{O}_3$  materials have four polymorphs phases such as  $\alpha\text{-Fe}_2\text{O}_3$  (hematite),  $\beta\text{-Fe}_2\text{O}_3$ ,  $\gamma\text{-Fe}_2\text{O}_3$  (maghemite) and  $\varepsilon\text{-Fe}_2\text{O}_3$  [17,18]. The differences of the phases are known from their originality, for examples, hematite and maghemite are naturally obtained and the other two of phases are synthesized in laboratory [19,20]. Among the phases,  $\gamma\text{-Fe}_2\text{O}_3$  is one of the chief interests. It is the second most common sustainable form of  $\text{Fe}_2\text{O}_3$ , known as completely oxidized magnetite. Maghemite has a high curie temperature, but has a lower saturation magnetization at room temperature and a supermagnetism property that makes it quite efficient in removing heavy metal pollutants from water [21,22]. Moreover, it is believed that  $\text{Fe}_2\text{O}_3$  can improve and provide better mechanical properties to chitosan [23].

Accumulation of heavy metals in water and food production, primarily mercury (Hg) is the most hazardous heavy-metal pollutants even at a very low concentration. The most toxic chemical forms of Hg are ionic Hg ( $\text{Hg}^{2+}$ ), causes serious damage to human health such as brain damage, immune dysfunction and paralysis [24–26]. Therefore, the removal and detection of  $\text{Hg}^{2+}$  in the aqueous environment are of great significance [27–31]. Among the existing optical techniques to detect  $\text{Hg}^{2+}$  are colorimetric, fluorescent, chemosensor, electrochemiluminescence (ECL) and photoluminescent (PL) [32–34]. Though these techniques are widely used, they encounter from many drawbacks, such as high instrument operating costs, repetitive pretreatment procedures and long initiation times [35].

Corresponding to the previous methods, surface plasmon resonance (SPR) proposed a cost-effective, label-free detection method for convenient usage, rapid detection and excellent sensitivity and selectivity to heavy metal ions [36–40]. Since enormous efforts devoted to creating sensors with high sensitivity to  $\text{Hg}^{2+}$  are greatly needed currently, selection of the metallic layer such as the gold layer is an important aid in producing higher sensor sensitivity in SPR [41]. Over the last decade, the surface SPR technique has emerged as an effective optical technique for various applications including detection of heavy metal ions [42–51]. Unfortunately, the main problem to detect optically the heavy metal ions solution is the similar refractive indices of heavy metal ions for lowest concentration, which eventually becomes the goal of researchers. Hence, many researchers have dedicated their time to develop chitosan-based materials onto SPR interfaces in lowering the detection limit of  $\text{Hg}^{2+}$ , specifically [52–54]. A recent study documented the utilization of polypyrrole-chitosan/nickel-ferrite nanoparticles as an active layer to a prism-based on SPR technique for  $\text{Hg}^{2+}$  sensing, which reached a limit of detection (LOD) as low as  $1.94\ \mu\text{M}$  [54]. Other recent studies using chitosan-based materials as sensing layers for the detection of  $\text{Hg}^{2+}$  by SPR are summarized in Table 1. It is of interest to further improve the LOD using chitosan-based SPR sensor.

**Table 1.** Chitosan based material by surface plasmon resonance (SPR) for the detection of  $\text{Hg}^{2+}$ .

Ref.	Sensing Layer	LOD
[38]	MMW chitosan (glutaraldehyde-crosslinked)	$2.49\ \mu\text{M}$
[52]	Polypyrrole-chitosan conducting polymer composite	$2.50\ \mu\text{M}$
[53]	Chitosan/graphene oxide	$0.50\ \mu\text{M}$
[54]	Polypyrrole-chitosan/nickel-ferrite nanoparticles	$1.94\ \mu\text{M}$

Ref.: reference. LOD: limit of detection.

To the best of our knowledge, the study for  $\text{Cs}/\gamma\text{-Fe}_2\text{O}_3$  composite to detect  $\text{Hg}^{2+}$  using the SPR technique is not reported yet. There is also a lack of studies on the structural and optical properties of these composites. Therefore, an effort was made to apply the chitosan/ $\gamma\text{-Fe}_2\text{O}_3$  thin film onto a thin gold surface, as a novel active layer for the SPR technique in sensing  $\text{Hg}^{2+}$  as low as nanomolar.

Besides, the studies of structural and optical properties of Cs/ $\gamma$ -Fe<sub>2</sub>O<sub>3</sub> thin film on the gold surface are also reported and explored.

## 2. Materials and Methods

### 2.1. Reagent and Materials

The Fe<sub>2</sub>O<sub>3</sub> was purchased from R&M Marketing, Essex, U.K. The medium molecular weight chitosan and acetic acid were purchased from Aldrich (Saint Louis, MO, USA). Standard solution of Hg<sup>2+</sup> with concentration of 1000 ppm was purchased from Merck (Darmstadt, Germany).

### 2.2. Preparation of Chemical

Firstly, 50 mL distilled water was added into Fe<sub>2</sub>O<sub>3</sub> (4 mg/mL). Then 10 mL of NH<sub>3</sub> (25%) and 0.615 mg of ethylenediaminetetra acetic acid (EDTA) was added as precipitation agent and as capping agent to the solution with stirring respectively. The reaction was allowed to proceed for 1 h at 50 °C with constant stirring. Finally, the black precipitate of nano-Fe<sub>2</sub>O<sub>3</sub>-EDTA formed and it was rinsed with distilled water and left to dry 80 °C for 3 h. For chitosan preparation, 1% acetic acid was prepared by diluting stock 1 mL acetic acid with deionized water in 100 mL volumetric flask. Next, 400 mg medium molecular weight chitosan that was acquired from Aldrich was dissolved in 50 mL of 1% aqueous acetic acid and the solution vigorously stirred to ensure powder chitosan dissolved completely. To produce the nanostructured chitosan/maghemite (Cs/Fe<sub>2</sub>O<sub>3</sub>) composites, 30 mg Fe<sub>2</sub>O<sub>3</sub> capped EDTA was dispersed in 10 mL of 0.1% chitosan solution and sonicated in room temperature for 15 min. The Hg<sup>2+</sup> standard solution with a concentration of 1000 ppm was diluted with deionized water to produce Hg<sup>2+</sup> solutions with concentrations of 0.01, 0.05, 0.08, 0.1 and 0.5 ppm [55,56].

### 2.3. Preparation of Thin Film

To begin, glass slips (24 mm × 24 mm × 0.1 mm, Menzel-Glaser, Braunschweig, Germany), as a substrate, were coated with a thin layer of gold with thickness 50 nm using SC7640 sputter coater [57]. Next, approximately 0.55 mL of the chitosan, Fe<sub>2</sub>O<sub>3</sub> and Cs/Fe<sub>2</sub>O<sub>3</sub> composites solution was set separately on the surface of the gold coated glass slip. Then the glass slips were spun at 6000 rev min for 30 s using the Specialty Coating System, P-6708D (Inc. Medical Devices, Indianapolis, IN, USA) to produce the chitosan, Fe<sub>2</sub>O<sub>3</sub> and Cs/Fe<sub>2</sub>O<sub>3</sub> composites thin films.

### 2.4. Instrumental

Fourier transform infrared (FTIR) spectra for each surface modification of thin films were recorded in the transmittance mode using a Perkin-Elmer spectrophotometer (Waltham, MA, USA) under the wavelength range 400–4000 cm<sup>-1</sup>. The absorbance spectra of the films were recorded from 200 to 500 nm using UV-Vis-NIR spectroscopy (UV-3600 Shimadzu, Kyoto, Japan). The optical band gap energy was calculated using the data obtained. Atomic force microscopy (AFM) analysis was carried out using Qscope 250, Qesant Instrument Corporation (Qesant, CA, USA) in intermittent mode to study the topography and height of Cs/Fe<sub>2</sub>O<sub>3</sub> thin film. An optical-based sensing method based on surface plasmon resonance (SPR) was designed to identify the potential of the Cs/Fe<sub>2</sub>O<sub>3</sub> thin film to detect Hg<sup>2+</sup>. Figure 1 shows the schematic diagram of the SPR instrument setup [58–61]. The SPR experiment was carried out by inserting Hg<sup>2+</sup> solutions with different concentration varied from 0.01 to 0.5 ppm. It was injected one after another into the cell to bind with Cs/Fe<sub>2</sub>O<sub>3</sub> thin film coated onto gold surface thin film. The SPR curve and resonance angle for all concentrations was monitored and recorded.

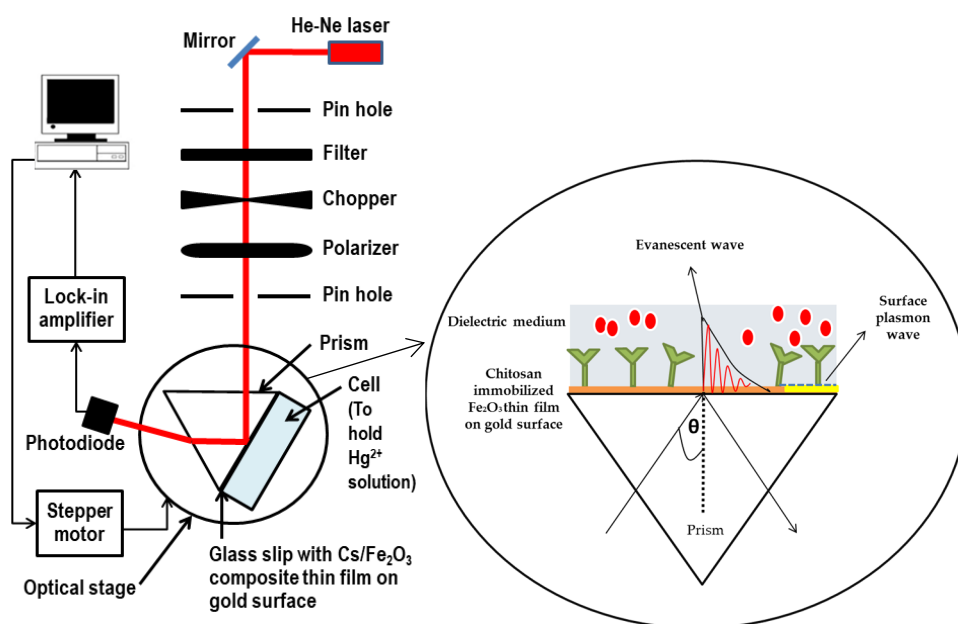


Figure 1. Optical setup of surface plasmon resonance spectroscopy.

### 3. Results and Discussion

#### 3.1. FTIR Analysis

FTIR spectroscopy was used to identify the functional groups existed in Cs/Fe<sub>2</sub>O<sub>3</sub> thin film. The spectrum of chitosan, Fe<sub>2</sub>O<sub>3</sub> and Cs/Fe<sub>2</sub>O<sub>3</sub> thin films in the range of 450–4000 cm<sup>-1</sup> are represented in Figure 2. From the FTIR spectrum of chitosan thin film, the broad absorption band at 3386.43 cm<sup>-1</sup> can be appointed to the stretching vibration of O–H. A weaker band found at 2901.26 cm<sup>-1</sup> can be attributed to C–H stretching in chitosan. Another absorption band at 1655.48 cm<sup>-1</sup> was associated with the presence of the C=O stretching bond. There is an absorption peak at 1084.47 cm<sup>-1</sup> that corresponds to the C–O group, which indicates the presence of the –COOH group in chitosan thin film. Two more bands at 500.76 cm<sup>-1</sup> and 458.22 cm<sup>-1</sup> were assigned to the C–C bond and C–N bond respectively. This finding is well aligned to the previous study by Anas et al. [62].

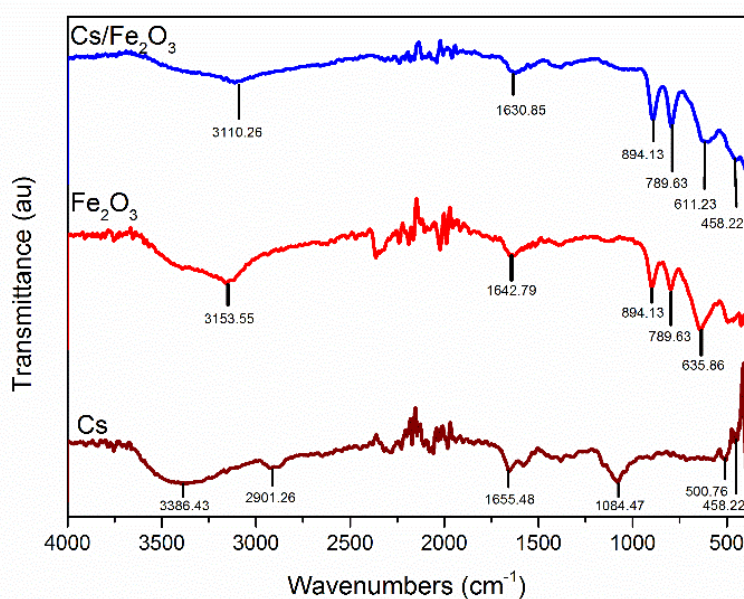


Figure 2. FTIR spectrum for chitosan, Fe<sub>2</sub>O<sub>3</sub> and Cs/Fe<sub>2</sub>O<sub>3</sub> thin films.

Next, a particular major peak in the  $\text{Fe}_2\text{O}_3$  thin film was identified with the degree of cation vacancy, ordering between octahedral Fe cation and O atoms [63]. The absorption peak at  $789.63\text{ cm}^{-1}$  is a characteristic of maghemite Fe–O stretching vibrations particles. This peak is solely attributed to the high degree of cationic vacancy ordering [64]. The broad band characteristic for bending vibration of water adsorbed on the maghemite's surface is at  $2078.99\text{ cm}^{-1}$ . The intense bands at  $1642.79\text{ cm}^{-1}$  and  $3153.55\text{ cm}^{-1}$  were then assigned to  $\text{CO}_2$  vibration and O–H vibrations, respectively, ratifying the presence of surface  $\gamma\text{-Fe}_2\text{O}_3$  hydroxyl groups.

In the spectrum of  $\text{Cs/Fe}_2\text{O}_3$ , the chitosan does not provide clear absorption bands at a lower wavenumber. This is due to the low percentage of chitosan compared to maghemite in the synthesization process. However, the presence of chitosan can be observed based on the intensity peak. The peak intensity of  $\text{Cs/Fe}_2\text{O}_3$  clearly increased after the sorption of chitosan and  $\text{Fe}_2\text{O}_3$ , i.e., at C–H stretching ( $458.22\text{ cm}^{-1}$ ), C–C bond ( $611.23\text{ cm}^{-1}$ ) and O=C=O stretching ( $1630.85\text{ cm}^{-1}$ ). An increase in the peak intensity usually indicates an increase in the sum of the functional group (per unit volume) associated with the molecular bond [65]. On the other hand, a strong absorption band was observed at  $789.63\text{ cm}^{-1}$ , confirmed the presence of Fe–O as the main phase of the  $\text{Fe}_2\text{O}_3$  and a band at  $3110.26\text{ cm}^{-1}$  that appointed to the O–H vibration of surface maghemite hydroxyl groups. Overall, the FTIR results showed the increasing peak intensity of  $\text{Cs/Fe}_2\text{O}_3$ , which confirmed the physical interaction of chitosan and  $\gamma\text{-Fe}_2\text{O}_3$  in those composites.

### 3.2. Surface Morphology

The in situ atomic force microscopy (AFM) measurements enable the chitosan,  $\text{Fe}_2\text{O}_3$  and  $\text{Cs/Fe}_2\text{O}_3$  adsorption on thin films to be visualized in real time. The AFM images illustrate the topographical in the thin films as shown in Figures 3–5. The topographical can be observed by various parameters that exist to quantify the root mean square (rms) roughness of a surface. The RMS roughness value can be calculated from the cross-sectional profile or a surface area [66]. The RMS roughness obtained by chitosan,  $\text{Fe}_2\text{O}_3$  and  $\text{Cs/Fe}_2\text{O}_3$  thin film were 1.4 nm, 47 nm and 37.3 nm, respectively. The magnitude decreased in RMS roughness of  $\text{Cs/Fe}_2\text{O}_3$  thin film compared to  $\text{Fe}_2\text{O}_3$  thin film attributable to the association of two materials, which are chitosan and  $\text{Fe}_2\text{O}_3$ . The roughness implies that a smoothening mechanism by surface diffusion [67]. This result indicates that the presence of chitosan can enhance the surface of the thin film. The roughness introduced in the nanostructured maghemite in chitosan thin film intended appropriate form to enhance the thin film as sensing element [68]. This result is in line with the FTIR data, proving the presence of maghemite and chitosan in the  $\text{Cs/Fe}_2\text{O}_3$  thin film based on the RMS roughness.

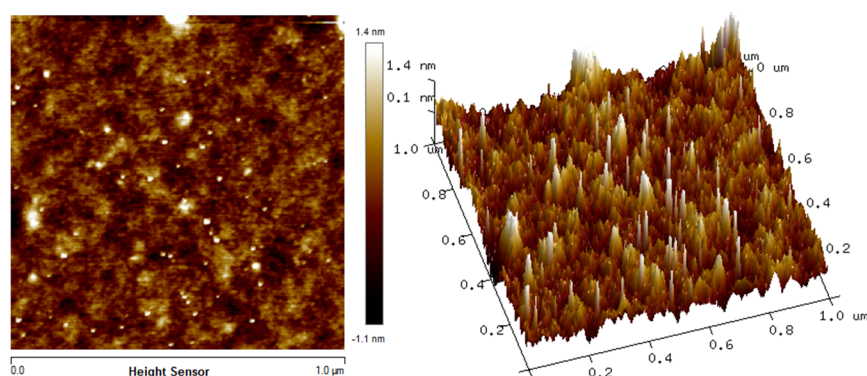


Figure 3. Atomic force microscopy (AFM) image of chitosan thin film.

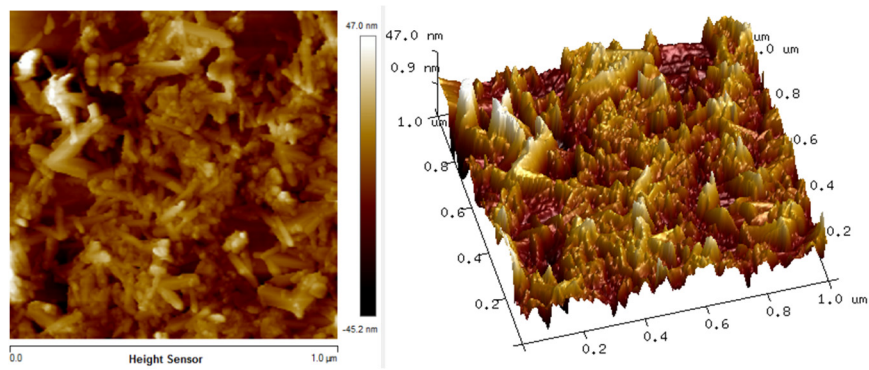


Figure 4. AFM image of Fe<sub>2</sub>O<sub>3</sub> thin film.

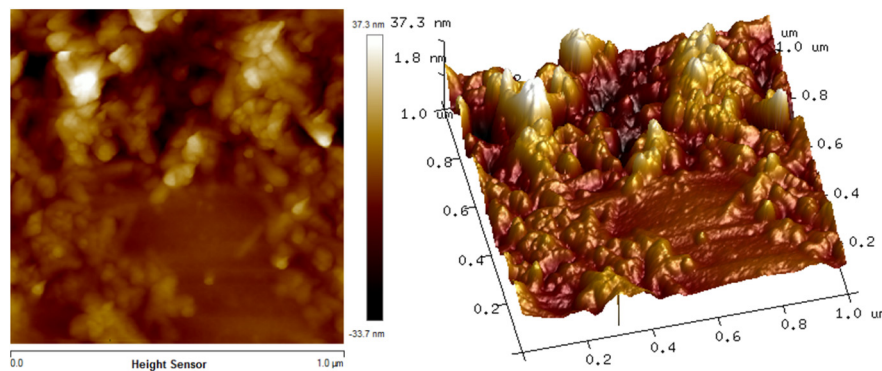


Figure 5. AFM image of Cs/Fe<sub>2</sub>O<sub>3</sub> thin film.

### 3.3. Optical Studies

For the optical properties, the absorbance spectrum of the thin films was observed and measured at wavelength from 250 to 500 nm. The UV-Vis results of chitosan, Fe<sub>2</sub>O<sub>3</sub> and Cs/Fe<sub>2</sub>O<sub>3</sub> thin films are shown in Figure 6 it can be spotted that all of the thin film has diverse value of absorbance. From the graph, the absorbance spectra of Cs and Fe<sub>2</sub>O<sub>3</sub> thin films were slightly higher as compared to the Cs/Fe<sub>2</sub>O<sub>3</sub> thin film. The maximum absorption wavelength can be observed at 260–300 nm. The absorption peak about 300 nm corresponds to  $\pi \rightarrow \pi^*$  transitions of C=O [69,70].

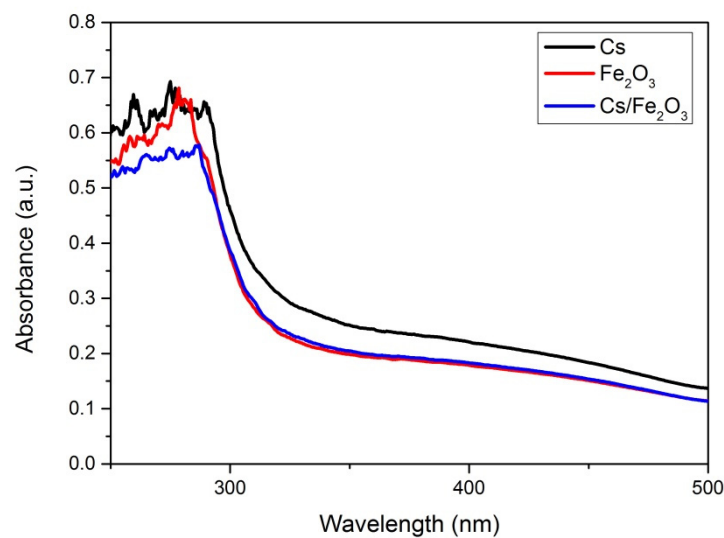


Figure 6. Absorbance spectrum chitosan, Fe<sub>2</sub>O<sub>3</sub> and Cs/Fe<sub>2</sub>O<sub>3</sub> thin films.

The UV-Vis absorbance spectrum was then quantitative analyzed based on the Beer–Lambert law theory. This law refers to a relation between the attenuation of light by a material and its properties, which the monochromatic light (single wavelength) is travelling. Since the amount of the emitted radiation intensity is only dependent on the thickness,  $t$  and concentration of the solution, the absorbance,  $A$  of the samples can be collected at a single wavelength, as follows [62]:

$$A = \log_{10} \frac{I_0}{I_t} \quad (1)$$

The transmittance,  $T$  of sample is given by the ratio of intensities of the presence  $I_t$  and the absence  $I_0$  of the sample:

$$T = \frac{I_t}{I_0} \quad (2)$$

Thus, the absorbance and transmittance can be related by:

$$A = -\log_{10} T \quad (3)$$

Apart from the absorbance, absorbance coefficient is a useful parameter to compare samples with varying thickness. The sample thickness was obtained by using atomic force microscopy. The absorbance coefficient,  $\alpha$  (in unit of  $\text{m}^{-1}$ ) is given by:

$$\alpha = 2.303 \frac{A}{t} \quad (4)$$

where  $t$  is the thickness of sample in unit of m. The absorbance coefficient and optical band gap can be related by:

$$\alpha = \frac{k(h\nu - E_g)^n}{h\nu} \quad (5)$$

Rearranging Equation (5) gives:

$$(\alpha h\nu)^{1/n} = k(h\nu - E_g) \quad (6)$$

where  $h\nu$  is the photon energy,  $h$  is Planck's constant,  $E_g$  is the optical band gap,  $k$  is constant and  $n$  is the transition states, i.e., direct or indirect transitions. Direct transition is transition in which a photon excites an electron from the valence band to the conduction band directly if the momentum of electrons and holes is the same in both bands (conduction and valence). On the other hand, indirect transition is a photon cannot be emitted because the electron must pass through an intermediate state and transfer momentum to the crystal lattice. From these, it can be concluded that the absorption in the thin films corresponds to a direct energy gap. For direct transition,  $n = 1/2$  and this value is substituted in Equation (6) and becomes:

$$(\alpha h\nu)^{1/n} = k(h\nu - E_g) \quad (7)$$

To evaluate the optical band gap,  $E_g$  of the chitosan,  $\text{Fe}_2\text{O}_3$  and  $\text{Cs}/\text{Fe}_2\text{O}_3$  thin films, the graphs of  $(\alpha h\nu)^2$  against  $h\nu$  are plotted as shown in Figures 7–9, respectively. As a result, the intersection of straight line on the edge was obtained, indicating the direct transition of the optical band gap [71]. The calculated values of the optical band gap were 4.073 eV, 4.078 eV and 4.013 eV for chitosan,  $\text{Fe}_2\text{O}_3$  and  $\text{Cs}/\text{Fe}_2\text{O}_3$  thin films respectively (with the corresponding error of  $\pm 0.001$  eV) [72,73]. This result indicated the maghemite had a band gap energy of 4.078 eV, which was higher than to the 2 eV bulk [64]. This might be due to the structure defects, that have changed the phase, strain and size of nanoparticles during heat treatment that led to the increase of band gap [74]. When  $\text{Fe}_2\text{O}_3$  added on chitosan, the band gap became lower as compared to the individual band gap. It can be due to the increased of crystallite size attributed to the confinement effects that related to the rise amount of orbitals participating in the formation of valence bands and covalent bands through orbital overlap [75].

Thus, this showed that defects and confinement effects have a huge impact on the optical properties of a composite.

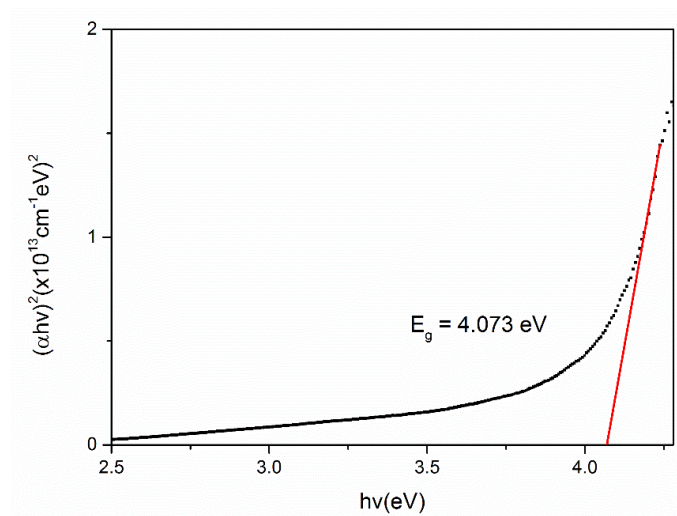


Figure 7. Optical band gap for chitosan thin film.

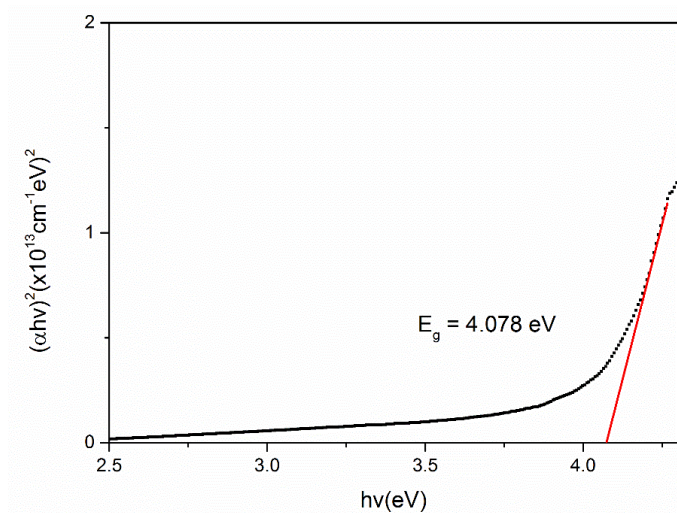


Figure 8. Optical band gap for Fe<sub>2</sub>O<sub>3</sub> thin film.

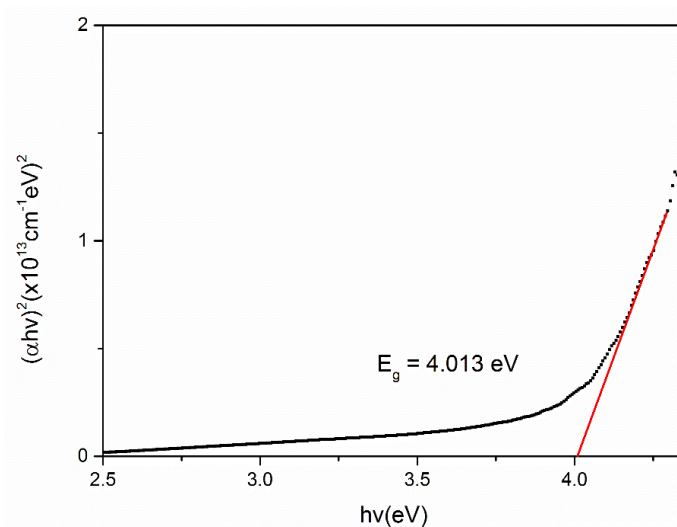
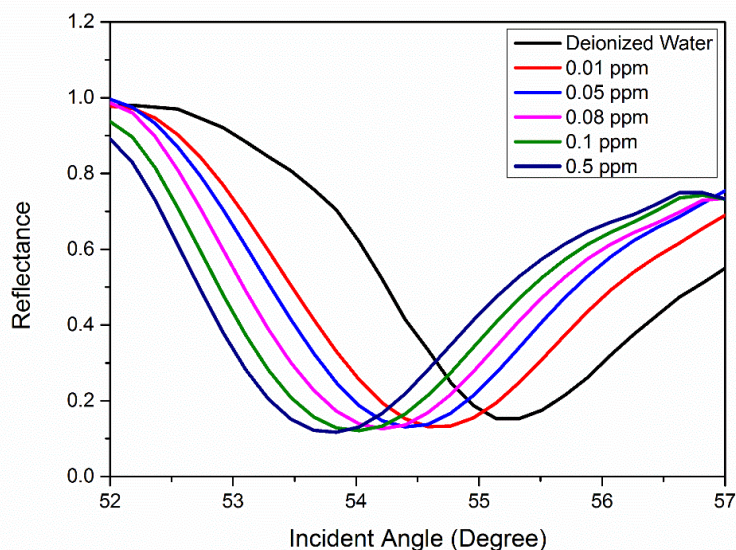


Figure 9. Optical band gap for Cs/Fe<sub>2</sub>O<sub>3</sub> thin film.

### 3.4. Optical-Based Sensing of $\text{Hg}^{2+}$

The optical sensing based on surface plasmon resonance (SPR) phenomenon was conducted by using  $\text{Cs}/\text{Fe}_2\text{O}_3$  thin film to identify the SPR angle for deionized water as a control experiment. The SPR angle of  $55.225^\circ$  was further applied to compare the SPR angle for different concentration of  $\text{Hg}^{2+}$  solution ranged from 0.01 to 0.5 ppm. The SPR reflectively curves for  $\text{Cs}/\text{Fe}_2\text{O}_3$  thin film in contact with the different concentration of  $\text{Hg}^{2+}$  are shown in Figure 10. It can be seen that the SPR curves of  $\text{Hg}^{2+}$  solution shifted from 0 to 0.5 ppm as compared with the deionized water SPR curve. The SPR angle for 0.01, 0.05, 0.08, 0.1 and 0.5 ppm of  $\text{Hg}^{2+}$  were  $54.615^\circ$ ,  $54.398^\circ$ ,  $54.212^\circ$ ,  $54.027^\circ$  and  $53.836^\circ$ , respectively, with the corresponding error of  $\pm 0.001^\circ$  (the resolution of the stepping motor of the SPR). Overall, it was observed that the SPR shifted to the left with increasing concentration of  $\text{Hg}^{2+}$  solution. This finding can be attributed to the increase in binding between analyte–ligand, which resulted in the change of refractive index as well as the thickness of the  $\text{Cs}/\text{Fe}_2\text{O}_3$  sensing layer [76–79]. Hence it is confirmed that  $\text{Cs}/\text{Fe}_2\text{O}_3$  thin film has an affinity with  $\text{Hg}^{2+}$  and can be integrated with SPR optical-based sensing method for detection of  $\text{Hg}^{2+}$ .



**Figure 10.** SPR curves for  $\text{Cs}/\text{Fe}_2\text{O}_3$  thin film in contact with deionized water and  $\text{Hg}^{2+}$  solution with a concentration of 0.01–0.5 ppm.

## 4. Conclusions

In this study, a  $\text{Cs}/\text{Fe}_2\text{O}_3$  thin film was successfully developed using the spin coating technique. The functional groups analysis from the FTIR results confirmed the correlation between chitosan and  $\gamma\text{-Fe}_2\text{O}_3$ , with the peak intensity of  $\text{Cs}/\text{Fe}_2\text{O}_3$  clearly increasing after the sorption of chitosan and  $\text{Fe}_2\text{O}_3$  at C–H stretching, C–C bond and O=C=O stretching. Next, the AFM result showed that the thin film was homogenous when the surface of chitosan on the thin film was covered by  $\text{Fe}_2\text{O}_3$ . Besides, the UV-Vis results confirmed that the  $\text{Cs}/\text{Fe}_2\text{O}_3$  thin film had the lowest absorbance value compared its individual thin films with an optical band gap of 4.013 eV. The incorporation  $\text{Cs}/\text{Fe}_2\text{O}_3$  thin film with the optical-based sensing method using the surface plasmon resonance technique provided positive response to the  $\text{Hg}^{2+}$  solution of different concentrations. This result demonstrated the enormous ability of  $\text{Cs}/\text{Fe}_2\text{O}_3$  thin film for optical sensing of  $\text{Hg}^{2+}$  as low as 0.01 ppm.

**Author Contributions:** Conceptualization, methodology, writing—original draft preparation, N.I.M.F.; validation, supervision, writing—review and editing, funding acquisition, Y.W.F.; investigation, formal analysis, N.A.S.O.; software, S.S.; visualization, W.M.E.M.M.D. and H.S.H.; resources, M.N. All authors have read and agreed to the published version of the manuscript.

**Funding:** This research was funded and supported by the Ministry of Education Malaysia through the Fundamental Research Grant Scheme (FRGS) (FRGS/1/2019/STG02/UPM/02/1) and Putra Grant Universiti Putra Malaysia.

**Acknowledgments:** The authors acknowledged the laboratory facilities provided by the Institute of Advanced Technology, Department of Physics, and Department of Chemistry, Universiti Putra Malaysia.

**Conflicts of Interest:** The authors declare no conflict of interest.

## References

1. Iwan, A.; Sek, D. Processible polyazomethines and polyketanils: From aerospace to light-emitting diodes and other advanced applications. *Prog. Polym. Sci.* **2008**, *33*, 289–345. [[CrossRef](#)]
2. Fen, Y.W.; Yunus, W.M.M.; Talib, Z.A.; Yusof, N.A. X-ray photoelectron spectroscopy and atomic force microscopy studies on crosslinked chitosan thin film. *Int. J. Phys. Sci.* **2011**, *6*, 2744–2749.
3. Martino, A.D.; Sittinger, M.; Risbud, M.V. Chitosan: A versatile biopolymer for orthopaedic tissue-engineering. *Biomaterials* **2005**, *26*, 5983–5990. [[CrossRef](#)]
4. Prashanth, K.V.H.; Tharanathan, R.N. Chitin/chitosan: Modifications and their unlimited application potential an-overview. *Trends Food Sci. Technol.* **2007**, *18*, 117–131. [[CrossRef](#)]
5. Divya, K.; Jisha, M.S. Chitosan nanoparticles preparation and applications. *Environ. Chem Lett.* **2017**, *16*, 101–112. [[CrossRef](#)]
6. Zargar, V.; Asghari, M.; Dashti, A. A review on chitin and chitosan polymers: Structure, chemistry, solubility, derivatives, and applications. *Chem. Bio. Eng.* **2015**, *2*, 204–226. [[CrossRef](#)]
7. Zhang, J.; Xia, W.; Liu, P.; Cheng, Q.; Tahirou, T.; Gu, W.; Li, B. Chitosan modification and pharmaceutical/biomedical applications. *Mar. Drugs* **2010**, *8*, 1962–1987. [[CrossRef](#)]
8. Fen, Y.W.; Yunus, W.M.M.; Yusof, N.A.; Ishak, N.S.; Omar, N.A.S.; Zainudin, A.A. Preparation, characterization and optical properties of ionophore doped chitosan biopolymer thin film and its potential application for sensing metal ion. *Optik* **2015**, *126*, 4688–4692. [[CrossRef](#)]
9. Ahmed, T.A.; Aljaeid, B.M. Preparation, characterization and potential application of chitosan, chitosan derivatives and chitosan metal nanoparticles in pharmaceutical drug delivery. *Drug Des. Devel. Ther.* **2016**, *10*, 483–507. [[CrossRef](#)]
10. Zhao, D.; Yu, S.; Sun, B.; Gao, S.; Guo, S.; Zhao, K. Biomedical applications of chitosan and its derivative nanoparticles. *Polymers* **2018**, *10*, 462. [[CrossRef](#)]
11. Saleviter, S.; Fen, Y.W.; Omar, N.A.; Zainudin, A.A.; Daniyal, W.M.E.M.M. Optical and structural characterization of immobilized 4-(2-pyridylazo) resorcinol in chitosan-graphene oxide composite thin film and its potential for Co<sup>2+</sup> sensing using surface plasmon resonance technique. *Results Phys.* **2018**, *11*, 118–122. [[CrossRef](#)]
12. Shukla, S.K.; Mishra, A.K.; Arotiba, O.A.; Mamba, B.B. Chitosan-based nanomaterials: A state-of-the-art review. *Int. J. Biol. Macromol.* **2013**, *59*, 46–58. [[CrossRef](#)] [[PubMed](#)]
13. Zainudin, A.A.; Fen, Y.W.; Yusof, N.A.; Al-Rekabi, S.H.; Mahdi, M.A.; Omar, N.A.S. Incorporation of surface plasmon resonance with novel valinomycin doped chitosan-graphene oxide thin film for sensing potassium ion. *Spectrochim. Acta A Mol. Biomol. Spectrosc.* **2018**, *191*, 111–115. [[CrossRef](#)] [[PubMed](#)]
14. Hassanein, A.; Salahuddin, N.; Matsuda, A.; Kawamura, G.; Elfiky, M. Fabrication of biosensor based on chitosan-ZnO/Polypyrrole nanocomposite modified carbon paste electrode for electroanalytical application. *Mater. Sci. Eng. C* **2017**, *80*, 494–501. [[CrossRef](#)] [[PubMed](#)]
15. Saleviter, S.; Fen, Y.W.; Daniyal, W.M.E.M.M.; Abdullah, J.; Sadrolhosseini, A.R.; Omar, N.A.S. Design and analysis of surface plasmon resonance optical sensor for determining cobalt ion based on chitosan-graphene oxide decorated quantum dots-modified gold active layer. *Opt. Express* **2019**, *27*, 32294–32307. [[CrossRef](#)]
16. Mariani, F.Q.; Borth, K.W.; Müller, M.; Dalpasquale, M.; Anaissi, F.J. Sustainable innovative method to synthesize different shades of iron oxide pigments. *Dyes Pigments* **2017**, *137*, 403–409. [[CrossRef](#)]
17. Machala, L.; Zboril, R.; Gedanken, A. Amorphous Iron(III) Oxide- A review. *Phys. Chem. B* **2007**, *111*, 4003–4018. [[CrossRef](#)]
18. Machala, L.; Tucek, J.; Zboril, R. Polymorphous transformations of nanometric iron(III) oxide: A review. *Chem. Mater.* **2011**, *23*, 3255–3272. [[CrossRef](#)]

19. Zboril, R.; Mashlan, M.; Petridis, D. Iron(III) oxides from thermal processes- synthesis, structural, and magnetic properties, mossbauer spectroscopy characterization and applications. *Chem. Mater.* **2002**, *14*, 969–982. [[CrossRef](#)]
20. Al-Rekabi, S.H.; Kamil, Y.M.; Bakar, M.H.A.; Fen, Y.W.; Lim, H.N.; Kanagesan, S.; Mahdi, M.A. Hydrous ferric oxide-magnetite-reduced graphene oxide nanocomposite for optical detection of arsenic using surface plasmon resonance. *Opt. Laser Technol.* **2019**, *111*, 417–423. [[CrossRef](#)]
21. Kharisov, B.I.; Dias, H.V.; Kharissova, O.V. Mini-Review: Ferrite nanoparticles in the catalysis. *Arab. J. Chem.* **2019**, *12*, 1234–1246. [[CrossRef](#)]
22. Usman, U.A.; Yusoff, I.; Raoov, M.; Hodgkinson, J. The economic potential of the African iron-ore tailings: Synthesis of magnetite for the removal of trace metals in groundwater—A review. *Environ. Earth Sci.* **2019**, *615*, 1–22. [[CrossRef](#)]
23. Lapo, B.; Demey, H.; Zapata, J.; Romero, C.; Sastre, A.M. Sorption of Hg(II) and Pb(II) ions on chitosan-Iron(III) from aqueous solutions: Single and binary systems. *Polymers* **2018**, *10*, 367. [[CrossRef](#)] [[PubMed](#)]
24. Genchi, G.; Sinicropi, M.S.; Carocci, A.; Lauria, G. Mercury exposure and heart diseases. *Int. J. Environ. Res. Public Health* **2017**, *14*, 74. [[CrossRef](#)]
25. Li, P.; Feng, X.B.; Qiu, G.L.; Shang, L.H.; Li, Z.G. Mercury pollution in Asia: A review of the contaminated sites. *J. Hazard. Mater.* **2009**, *168*, 591–601. [[CrossRef](#)]
26. Reilly, S.B.; Lettmeier, B.; Matteucci, R.; Beinhoff, C.; Siebert, U.; Drasch, V. Mercury as a serious health hazard for children in gold mining areas. *Environ. Res.* **2008**, *107*, 89–97.
27. Miretzky, P.; Cirelli, A.F. Hg(II) removal from water by chitosan and chitosan derivatives: A review. *J. Hazard. Mater.* **2009**, *167*, 10–23. [[CrossRef](#)]
28. Roshidi, M.D.A.; Fen, Y.W.; Omar, N.A.S.; Saleviter, S.; Daniyal, W.M.E.M.M. Optical studies of graphene oxide/poly(amidoamine) dendrimer composite thin film and its potential for sensing Hg<sup>2+</sup> using surface plasmon resonance spectroscopy. *Sens. Mater.* **2018**, *31*, 1147–1156. [[CrossRef](#)]
29. Ramdzan, N.S.M.; Fen, Y.W.; Omar, N.A.S.; Saleviter, S.; Zainudin, A.A. Optical and surface plasmon resonance sensing properties for chitosan/carboxyl-functionalized graphene quantum dots thin film. *Optik* **2019**, *178*, 802–812. [[CrossRef](#)]
30. Fen, Y.W.; Yunus, W.M.M.; Moxsin, M.M.; Talib, Z.A.; Yusof, N.A. Surface plasmon resonance optical sensor for mercury ion detection by crosslinked chitosan thin film. *J. Optoelectron. Adv. Mater.* **2011**, *13*, 279–285.
31. Chen, Z.; Han, K.; Zhang, Y. Reflective fiber surface plasmon resonance sensor for high-sensitive mercury ion detection. *Appl. Sci.* **2019**, *9*, 1480. [[CrossRef](#)]
32. Uglov, A.N.; Bessmertnykh-Lemeune, A.; Guillard, R.; Averin, A.D.; Beletskaya, I.P. Optical methods for the detection of heavy metal ions. *Russ. Chem. Rev.* **2014**, *83*, 196–224. [[CrossRef](#)]
33. Tang, W.; Li, J.; Guo, Q.; Nie, G. An ultrasensitive electrochemiluminescence assay for Hg<sup>2+</sup> through graphene quantum dots and poly(5-formylindole) nanocomposite. *Sens. Actuators B Chem.* **2019**, *282*, 824–830. [[CrossRef](#)]
34. Wang, B.B.; Jin, J.C.; Xu, Z.Q.; Jiang, Z.W.; Li, X.; Jiang, F.L.; Liu, Y. Single-step synthesis of highly photoluminescent carbon dots for rapid detection of Hg<sup>2+</sup> with excellent sensitivity. *J. Colloid Interface Sci.* **2019**, *551*, 101–110. [[CrossRef](#)]
35. Xu, X.; Zhang, Y.; Wang, B.; Luo, L.; Xu, Z.; Tian, X. A novel surface plasmon resonance sensor based on a functionalized graphene oxide/molecularimprinted polymer composite for chiral recognition of L-tryptophan. *RSC Adv.* **2018**, *8*, 32538–32544. [[CrossRef](#)]
36. Kurihara, K.; Nakamura, K.; Suzuki, K. Asymmetric SPR sensor response curve-fitting equation for the accurate determination of SPR resonance angle. *Sens. Actuators B Chem.* **2002**, *86*, 49–57. [[CrossRef](#)]
37. Xue, T.; Qi, K.; Hu, C. Novel SPR sensing platform based on superstructure MoS<sub>2</sub> nanosheets for ultrasensitive detection of mercury ion. *Sens. Actuators B Chem.* **2019**, *284*, 589–594. [[CrossRef](#)]
38. Fen, Y.W.; Yunus, W.M.M.; Yusof, N.A. Detection of mercury and copper ions using surface plasmon resonance optical sensor. *Sens. Mater.* **2011**, *23*, 325–334.
39. Ramdzan, N.S.M.; Fen, Y.W.; Anas, N.A.A.; Omar, N.A.S.; Saleviter, S. Development of biopolymer and conducting polymer-based optical sensors for heavy metal ion detection. *Molecules* **2020**, *25*, 2548. [[CrossRef](#)]
40. Homola, J. Surface plasmon resonance sensors for detection of chemical and biological species. *Chem. Rev.* **2008**, *108*, 462–493. [[CrossRef](#)]

41. Lokman, N.F.; Azeman, N.H.; Suja, F.; Arsad, N.; Bakar, A.A. Sensitivity enhancement of Pb(II) ion detection in rivers using SPR-based Ag metallic layer coated with chitosan–graphene oxide nanocomposite. *Sensors* **2019**, *19*, 5159. [[CrossRef](#)] [[PubMed](#)]
42. Omar, N.A.S.; Fen, Y.W. Recent development of SPR spectroscopy as potential method for diagnosis of dengue virus E-protein. *Sens. Rev.* **2018**, *38*, 106–116. [[CrossRef](#)]
43. Fujii, E.; Koike, T.; Nakamura, K.; Sasaki, S.; Kurihara, K.; Citterio, D.; Suzuki, K. Application of an absorption-based surface plasmon resonance principle to the development of SPR ammonium ion and enzyme sensors. *Anal. Chem.* **2002**, *74*, 6106–6110. [[CrossRef](#)]
44. Eddin, F.B.K.; Fen, Y.W. Recent Advances in electrochemical and optical sensing of dopamine. *Sensors* **2020**, *20*, 1039.
45. Fen, Y.W.; Yunus, W.M.M. Surface plasmon resonance spectroscopy as an alternative for sensing heavy metal ions: A review. *Sens. Rev.* **2013**, *33*, 305–314.
46. Victoria, S. Application of surface plasmon resonance (SPR) for the detection of single viruses and single biological nano-objects. *J. Bacteriol. Parasitol.* **2012**, *3*, 1–3. [[CrossRef](#)]
47. Jia, Y.; Peng, Y.; Bai, J.; Zhang, X.; Cui, Y.; Ning, B.; Cui, J.; Gao, Z. Magnetic nanoparticle enhanced surface plasmon resonance sensor for estradiol analysis. *Sens. Actuators B Chem.* **2017**, *254*, 629–635. [[CrossRef](#)]
48. Daniyal, W.M.E.M.M.; Saleviter, S.; Fen, Y.W. Development of surface plasmon resonance spectroscopy for metal ion detection. *Sens. Mater.* **2018**, *30*, 2023–2038. [[CrossRef](#)]
49. Omar, N.A.S.; Fen, Y.W.; Saleviter, S.; Daniyal, W.M.E.M.M.; Anas, N.A.A.; Ramdzan, N.S.M.; Roshidi, M.D.A. Development of a graphene-based surface plasmon resonance optical sensor chip for potential biomedical application. *Materials* **2019**, *12*, 1928. [[CrossRef](#)]
50. Zhou, C.; Zou, H.; Li, M.; Sun, C.; Ren, D.; Li, Y. Fiber optic surface plasmon resonance sensor for detection of E. coli O157:H7 based on antimicrobial peptides and AgNPs-rGo. *Biosens. Bioelectron.* **2018**, *117*, 347–353. [[CrossRef](#)]
51. Anas, N.A.A.; Fen, Y.W.; Omar, N.A.S.; Daniyal, W.M.E.M.M.; Ramdzan, N.S.M.; Saleviter, S. Development of graphene quantum dots-based optical sensor for toxic metal ion detection. *Sensors* **2019**, *19*, 3850. [[CrossRef](#)] [[PubMed](#)]
52. Abdi, M.M.; Abdullah, L.C.; Sadrolhosseini, A.R.; Yunus, W.M.M.; Moxsin, M.F.; Tahir, P.M. Surface Plasmon Resonance Sensing Detection of Mercury and Lead Ions Based on Conducting Polymer Composite. *PLoS ONE* **2011**, *6*, 24578. [[CrossRef](#)] [[PubMed](#)]
53. Kamaruddin, N.H.; Bakar, A.A.A.; Mobarak, N.N.; Zan, M.S.D.; Arsad, N. Binding affinity of a highly sensitive Au/Ag/Au/chitosan-graphene oxide sensor based on direct detection of Pb<sup>2+</sup> and Hg<sup>2+</sup> ions. *Sensors* **2017**, *17*, 2277. [[CrossRef](#)]
54. Sadrolhosseini, A.R.; Naseri, M.; Rasyid, S.A. Polypyrrole-chitosan/nickel-ferrite nanoparticle composite layer for detecting heavy metal ions using surface plasmon resonance technique. *Opt. Laser Technol.* **2017**, *93*, 216–223. [[CrossRef](#)]
55. Fen, Y.W.; Yunus, W.M.M.; Yusof, N.A. Surface plasmon resonance optical sensor for detection of essential heavy metal ions with potential for toxicity: Copper, zinc and manganese ions. *Sens. Lett.* **2011**, *9*, 1704–1711. [[CrossRef](#)]
56. Daniyal, W.M.E.M.M.; Fen, Y.W.; Abdullah, J.; Sadrolhosseini, A.R.; Saleviter, S.; Omar, N.A.S. Exploration of surface plasmon resonance for sensing copper ion based on nanocrystalline cellulose-modified thin film. *Opt. Express* **2018**, *26*, 34880–34893. [[CrossRef](#)]
57. Saleviter, S.; Fen, Y.W.; Omar, N.A.S.; Zainudin, A.A.; Yusof, N.A. Development of optical sensor for determination of Co(II) based on surface plasmon resonance phenomenon. *Sens. Lett.* **2017**, *15*, 862–867. [[CrossRef](#)]
58. Fen, Y.W.; Yunus, W.M.M.; Yusof, N.A. Surface plasmon resonance optical sensor for detection of Pb<sup>2+</sup> based on immobilized p-tert-butylcalix[4]arene-tetrakis in chitosan thin film as an active layer. *Sens. Actuators B Chem.* **2012**, *171–172*, 287–293. [[CrossRef](#)]
59. Fen, Y.W.; Yunus, W.M.M. Characterization of the optical properties of heavy metal ions using surface plasmon resonance technique. *Opt. Photonics.* **2011**, *1*, 116–123. [[CrossRef](#)]
60. Fen, Y.W.; Yunus, W.M.M.; Talib, Z.A.; Yusof, N.A. Development of surface plasmon resonance sensor for determining zinc ion using novel active nanolayers as probe. *Spectrochim. Acta A Mol. Biomol. Spectrosc.* **2015**, *134*, 48–52. [[CrossRef](#)]

61. Roshidi, D.A.; Fen, Y.W.; Daniyal, W.M.E.M.M.; Omar, N.A.S.; Zulholinda, M. Structural and optical properties of chitosan–poly(amidoamine) dendrimer composite thin film for potential sensing  $Pb^{2+}$  using an optical spectroscopy. *Optik* **2019**, *185*, 351–358. [[CrossRef](#)]
62. Anas, N.A.A.; Fen, Y.W.; Omar, N.A.S.; Ramdzan, N.S.M.; Daniyal, W.M.E.M.M.; Saleviter, S.; Zainudin, A.A. Optical properties of chitosan/hydroxyl-functionalized graphene quantum dots thin film for potential optical detection of ferric(III) ion. *Opt. Laser Technol.* **2019**, *120*, 105724. [[CrossRef](#)]
63. Rajput, S.; Singh, L.P.; Pittman, C.U., Jr.; Mohan, D. Lead ( $Pb^{2+}$ ) and copper ( $Cu^{2+}$ ) remediation from water using superparamagnetic maghemite ( $\gamma-Fe_2O_3$ ) nanoparticles synthesized by Flame Spray Pyrolysis (FSP). *J. Colloid Interface Sci.* **2016**, *492*, 176–190. [[CrossRef](#)] [[PubMed](#)]
64. Nasser, A.M.B. Synthesis and characterization of maghemite iron oxide ( $\gamma-Fe_2O_3$ ) nanofibers: Novel semiconductor with magnetic feature. *J. Mater. Sci.* **2016**, *47*, 6237–6245.
65. Coates, J. *Encyclopedia of Analytical Chemistry*; John Wiley & Sons Ltd.: Chichester, NH, USA, 2006; pp. 10815–10837.
66. Zainudin, A.A.; Fen, Y.W.; Yusof, N.A.; Omar, N.A.S. Structural, optical and sensing properties of ionophore doped graphene based bionanocomposite thin film. *Optik* **2017**, *144*, 308–315. [[CrossRef](#)]
67. Vujtek, M.; Zboril, R.; Kubinek, R.; Mashlan, M. Ultrafine particles of iron(III) oxides by view of AFM–Novel route for study of polymorphism in nano-world. *Nanomaterials* **2003**, *3*, 1–8.
68. Daniyal, W.M.E.M.M.; Fen, Y.W.; Abdullah, J.; Saleviter, S.; Omar, N.A.S. Preparation and characterization of hexadecyltrimethyl-ammonium bromide modified nanocrystalline cellulose/graphene oxide composite thin film and its potential in sensing copper ion using surface plasmon resonance technique. *Optik* **2018**, *173*, 71–77. [[CrossRef](#)]
69. Rattana, T.; Chaiyakun, S.; Witit-anun, N.; Nuntawong, N.; Chindaudom, P. Preparation and characterization of graphene oxide nanosheets. *Procedia Eng.* **2012**, *32*, 759–764. [[CrossRef](#)]
70. Kumar, S.; Koh, J. Physiochemical and optical properties of chitosan based graphene oxide bionanocomposite. *Int. J. Biol. Macromol.* **2014**, *70*, 559–564. [[CrossRef](#)]
71. Abdulla, H.; Abbo, A. Optical and electrical properties of thin films of polyaniline and polypyrrole. *Int. J. Electrochem. Sci.* **2012**, *7*, 10666–10678.
72. Dhlamini, M.S.; Noto, L.L.; Mothudi, B.M.; Chithambo, M.; Mathevula, L.E. Structural and optical properties of sol-gel derived  $\alpha-Fe_2O_3$  nanoparticles. *J. Lumin.* **2017**, *192*, 879–887.
73. Al-Kuhaili, M.F.; Saleem, M.; Durrani, S.M.A. Optical properties of iron oxide ( $\alpha-Fe_2O_3$ ) thin films deposited by the reactive evaporation of iron. *J. Alloys Compd.* **2012**, *521*, 178–182. [[CrossRef](#)]
74. He, Y.P.; Miao, Y.M.; Li, C.R.; Wang, S.Q.; Cao, L.; Xie, S.S.; Yang, G.Z.; Zou, B.S.; Burda, C. Size and structure effect on optical transitions of iron oxide nanocrystals. *Rev. B Condens. Matter.* **2005**, *71*, 1–9. [[CrossRef](#)]
75. Deotale, A.J.; Nandedkar, R.V. Correlation between particle size, strain and band gap of iron oxide nanoparticles. *Mater. Today* **2016**, *3*, 2069–2076. [[CrossRef](#)]
76. Fen, Y.W.; Yunus, W.M.M.; Talib, Z.A. Analysis of  $Pb(II)$  ion sensing by crosslinked chitosan thin film using surface plasmon resonance spectroscopy. *Optik* **2013**, *124*, 126–133. [[CrossRef](#)]
77. Lokman, N.F.; Bakar, A.A.A.; Suja, F.; Abdullah, H.; Rahman, W.B.W.A.; Yaacob, M.H. Highly sensitive SPR response of Au/chitosan/graphene oxide nanostructured thin films toward  $Pb(II)$  ions. *Sens. Actuators B Chem.* **2014**, *195*, 459–466. [[CrossRef](#)]
78. Fen, Y.W.; Yunus, W.M.M. Utilization of chitosan-based sensor thin films for the detection of lead ion by surface plasmon resonance optical sensor. *IEEE Sens. J.* **2013**, *13*, 1413–1418. [[CrossRef](#)]
79. Fen, Y.W.; Yunus, W.M.M.; Yusof, N.A. Optical properties of crosslinked chitosan thin film as copper ion detection using surface plasmon resonance technique. *Opt. Appl.* **2011**, *41*, 999–1013.

